Optics & Laser Technology 75 (2015) 6–12

Contents lists available at ScienceDirect

Optics & Laser Technology

journal homepage: www.elsevier.com/locate/optlastec

Fabrication and analysis of tall-stepped mirror for use in static Fourier transform infrared spectrometer

Cheng Chen [a,b], Jingqiu Liang [a,*], Zhongzhu Liang [a], Jinguang Lü [a], Yuxin Qin [a], Chao Tian [a], Weibiao Wang [a]

[a] State Key Laboratory of Applied Optics, Changchun Institute of Optics, Fine Mechanics and Physics, Chinese Academy of Sciences, Changchun, Jilin 130033, China

[b] University of Chinese Academy of Sciences, Beijing 100039, China

ARTICLE INFO

Article history:
Received 25 March 2015
Received in revised form
8 June 2015
Accepted 12 June 2015
Available online 23 June 2015

Keywords:
Spectrometers
Micro-optical devices
Fabrication tolerance
Spectrum analysis

ABSTRACT

A method of "slope splicing" is proposed to build a tall-stepped mirror with high precision in a stepped-mirror-based static Fourier transform infrared spectrometer. The structural parameters were designed, and their errors were analyzed. We present the test results and an analysis of the combined effect of the errors on the recovered spectrum. The spectrum-constructing error of the constructed spectrum, 5.81%, meets the requirements for the system and suitable for realization of a miniaturized spectrometer. We performed experiments with the tall-stepped mirror to obtain the interferogram and spectrum of a silicon carbide light source. Further work is needed to optimize the capability of the system.

1. Introduction

Spectrometers are widely used in many fields, including chemical analysis, environmental monitoring, and space exploration. Fourier transform spectrometers (FTSs) are favored because of their high luminous flux and multi channel transmission capacity [1–3]. Most industrial FTSs are time-modulated and equipped with a moving plane mirror. However, the movement precision and system stability are still large problems [4]. A space-modulated FTS based on a Michelson interferometer with the two plane mirrors replaced by two stepped mirrors was proposed by Möller in 1992 [5,6] and studied at other institutions [7–9]. With advances in technology, miniaturized and lightweight FTSs became urgently necessary, and we proposed a micro static Fourier transform infrared (FTIR) spectrometer based on micro-optical electro-mechanical system (MOEMS) technology [10]. Compared with other micro FTSs, it has significant advantages of stability, a simplified configuration, and excellent repeatability because it has no moving components.

As the core components of FTIR spectrometer, two stepped mirrors play an important role in sampling the interferogram at different optical path differences (OPDs); the spectrum is then obtained through Fourier transform of the interferogram. However, the Fourier transform requires exactly equal sampling intervals, and the obtained spectrum is crucially sensitive to the sampling errors [11]. For a tall-stepped mirror (TSM), the step height error and sub-mirror width error produce nonuniform samples in the interferogram [12,13], and the sub-mirror angle error causes variation in the OPD [14]. Furthermore, the roughness of the reflecting surface will produce spectral artifacts. Therefore, the TSM requires a highly precise surface, which is difficult to manufacture [15].

Many technologies for fabricating a short-stepped mirror with step height 0.625 μm have been discussed in early research [15,16], whereas it is helpless to the taller steps. It has been difficult to build a TSM with a step height of 20 μm. In this paper, a simplicity and cost-effective method of building a TSM by "slope splicing" is proposed and realized. The errors in the structural parameters of the TSM, i.e., the step height, sub-mirror width, sub-mirror tilt angle, and roughness of the reflecting surface, were analyzed and tested, and their combined effects on the recovered spectrum were discussed. Finally, experiments were performed with the TSM used in the static FTIR spectrometer to obtain the interferogram and recovered spectrum for a silicon carbide light source.

2. Principle of the FTIR spectrometer

Fig. 1 shows a schematic drawing of the configuration of the static FTIR spectrometer, which is based on Michelson's interferometer with

* Corresponding author. Fax: +86 043186176920.
E-mail addresses: liangjq@ciomp.ac.cn (J. Liang), liangzz@ciomp.ac.cn (Z. Liang).

http://dx.doi.org/10.1016/j.optlastec.2015.06.010
0030-3992/

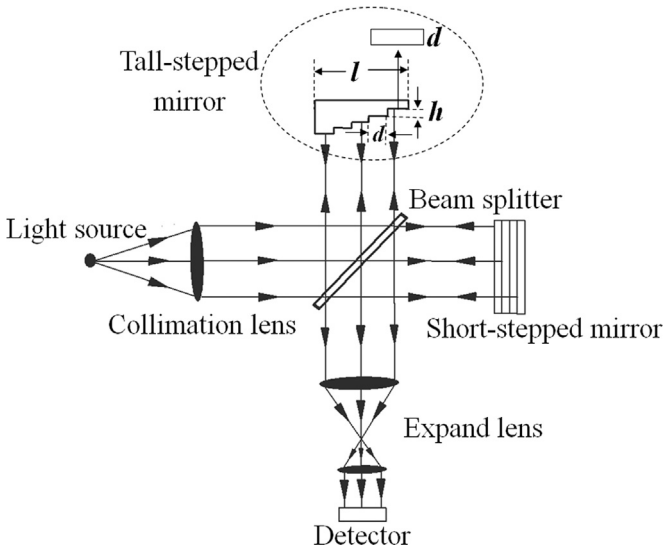

Fig. 1. Schematic drawing of configuration of the micro static FTIR spectrometer.

the two plane mirrors replaced by two crossed stepped mirrors each consisting of N steps. This paper focuses primarily on the TSM (dashed circle), where h is the step height, d is the sub-mirror width, and l and w are the effective length and width, respectively. The two stepped mirror heights are necessary to satisfy the Nyquist–Shannon sampling criterion and the principle of OPD continuity, i.e., that one tall step height corresponds to the sum of the steps of the short-stepped mirror. As a result, the system produces $N \times N$ samples with a uniform sampling interval of twice the step height of the short-stepped mirror. The interferometric function of a sample, which has been shown in [3], is

$$I(n, m) = \int_0^\infty B(\nu)\exp[j2\pi\nu\delta(n, m)]\mathrm{d}\nu. \tag{1}$$

$I(n, m)$ is the interferogram intensity at sample area (n, m), where n is the nth step of the TSM, and m is the mth step of the short-stepped mirror. $B(\nu)$ is the density of the power spectrum, ν is the spatial frequency of the optical signal, and $\delta(n, m)$ is the OPD on the spatial sampling area (n, m).

3. Design and error analysis of the TSM

3.1. Design

The structure of TSM is shown inside the dashed circle in Fig. 1. According to the Nyquist–Shannon sampling criterion, for the Nyquist frequency ν_{max}, the sampling frequency of the interferogram ν_{sample} must be greater than twice the greatest wavenumber. Thus, the sampling interval is smaller than half the minimum wavelength; i.e., $\Delta \le \lambda_{min}/2$. To obtain a spectral resolution R, the sampling length L must be greater than the reciprocal of R (*i.e.*, $L \ge 1/R$), and the number of sampling areas N must obey $N \ge L/\Delta$.

The working wavelength of the system ranges from 2.5 to 12 μm; the number of samples is 1024, and the step height of the short-stepped mirror is 0.625 μm. Thus, the number of steps N is 32, and the step height h of the TSM is 20 μm. Considering the effect of diffraction, the sub-mirror width d is 1 mm [4], the effective length is l, and the overall width w is 32 mm.

3.2. Error analysis

The limited machining and locating precision of the sub-mirror during the fabrication process can cause the step height, sub-mirror width, sub-mirror angle, and surface roughness to deviate from the ideal values [14]. We analyzed the resulting distortion in the recovered spectrum.

The real spectrum different from the ideal spectrum that we call "the spectrum-constructing error (SCE)" was defined as

$$\mathrm{SCE} = \frac{\sum_{k=0}^{N} \left|B_{\mathrm{real}}(k) - B_{\mathrm{ideal}}(k)\right|}{\sum_{k=0}^{N} B_{\mathrm{ideal}}(k)}, \tag{2}$$

where $B_{\mathrm{real}}(k)$ is the power of the real recovered spectrum, and $B_{\mathrm{ideal}}(k)$ is the power of the ideal spectrum [11].

Given that the additional OPD introduced by the structural parameter errors of TSM is $\Delta\delta(n)$, according to Eq. (1), the light intensity distribution of the interferogram obtained by the detector is

$$I(n, m) = \int_0^\infty B(v)\exp\{j2\pi v[2(Nn - m)h + \Delta\delta(n)]\}\mathrm{d}v. \tag{3}$$

The real recovered spectrum with the errors is then obtained via the fast Fourier transform (FFT) in Eq. (3).

For the nth step, the step height error is $x(n)$, the width error is $\varepsilon(n)$, and the tilt angle error is $\theta(n)$, as shown in Fig. 2. When we consider only the step height error, $\Delta\delta(n)$ is

$$\Delta\delta_x(n) = 2x(n), \tag{4}$$

the width error is

$$\Delta\delta_\varepsilon(n) = 2\varepsilon(n)\tan\ \Phi, \tag{5}$$

the tilt angle error is

$$\Delta\delta_\theta(n) = 2d\ \tan\ \theta(n), \tag{6}$$

and the three errors together are

$$\Delta\delta(n) = 2\{x(n) + \varepsilon(n)\tan\ \Phi + [d + \varepsilon(n)]\ \tan\ \theta(n)\}, \tag{7}$$

Figs. 3–6 show the SCE theoretical value vs. the standard deviation of the step height, sub-mirror width, sub-mirror tilt angle, and surface roughness, respectively, of the TSM. For each structural parameter error, the TSM was generated and the spectrum was constructed 1000 times, and the SCE of each structural parameter's standard deviation was obtained by taking the

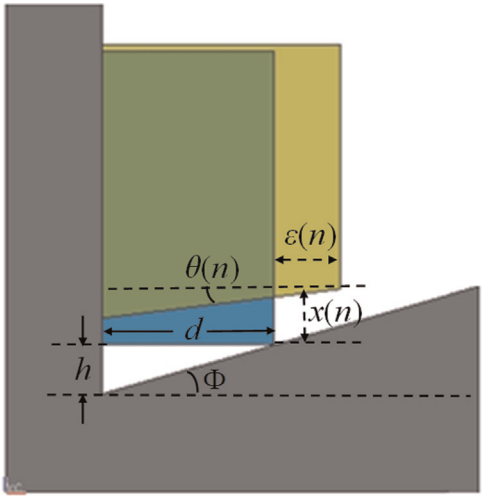

Fig. 2. Step height error, sub-mirror width error, and sub-mirror tilt angle error of nth step.

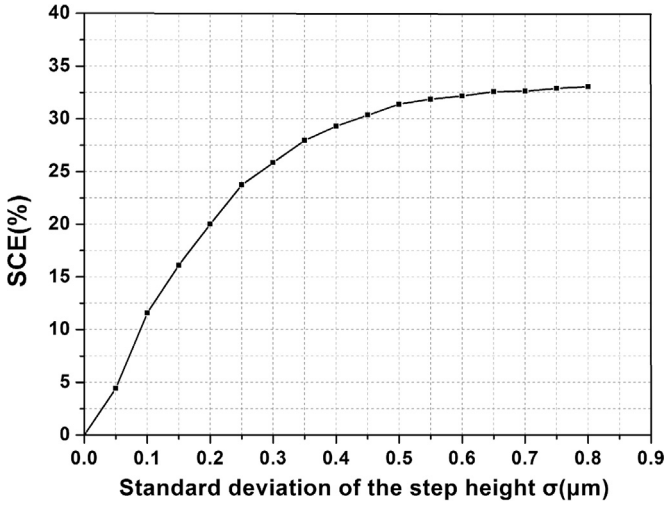

Fig. 3. SCE vs. the standard deviation of the step height.

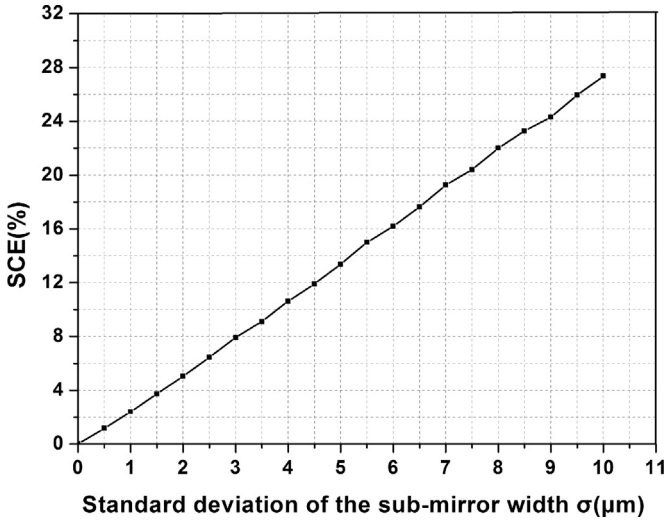

Fig. 4. SCE vs. the standard deviation of the sub-mirror width.

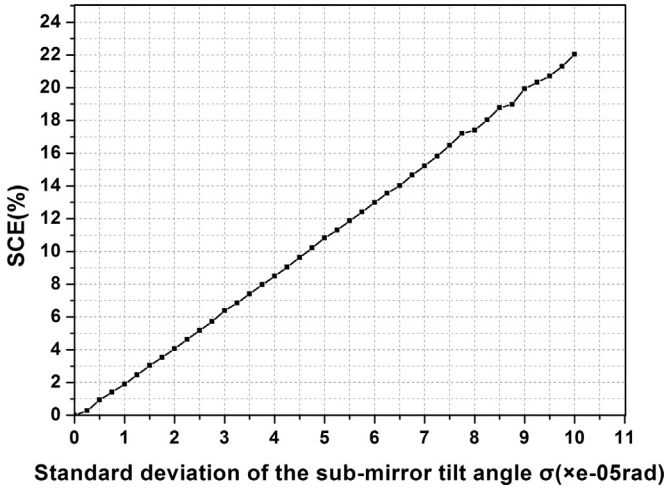

Fig. 5. SCE vs. the standard deviation of the sub-mirror tilt angle.

statistical average. Figs. 3 and 6 show that the standard deviations of the step height and roughness increase nonlinearly with increasing SCE. To achieve an SCE value of less than 10%, the standard deviations of the step height and roughness must be less

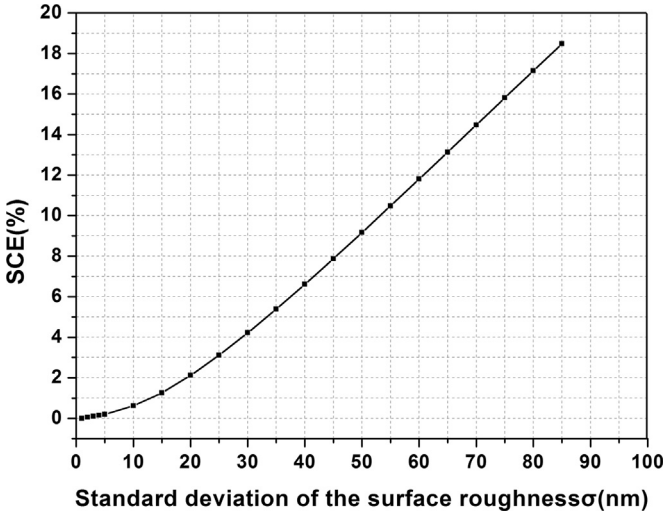

Fig. 6. SCE vs. the standard deviation of the surface roughness.

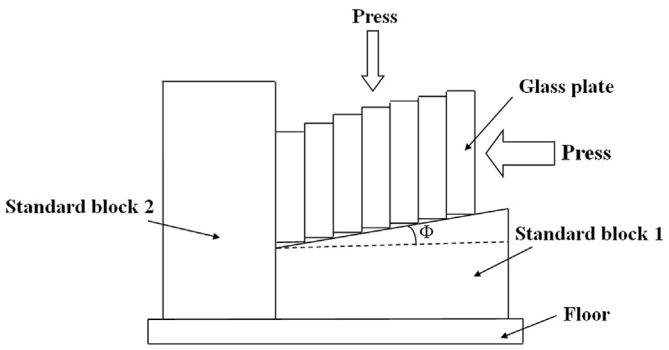

Fig. 7. Schematic drawing of slope splicing configuration.

than 0.08 μm and 50 nm, respectively. Figs. 4 and 5 show that the standard deviations of the sub-mirror width and sub-mirror tilt angle increase nearly linearly with increasing SCE. The standard deviations of the sub-mirror width and tilt angle should be less than 4 μm and 4.5×10^{-5} rad, respectively, to obtain an SCE value of less than 10%. These small values make it clear that highly precise manufacturing is needed.

4. Fabrication and test result analysis

4.1. Fabrication

For the TSM, each step height is 20 μm, so the total amount of height of 32 steps is 640 μm. If this TSM is fabricated with the methods such as the lithography-electroplating method, etching method, or conventional mechanical method, the surface quality, flatness and reproducibility of the steps will be declined, and cannot satisfy the high accuracy requirements of the optical system [7,8,15]. Thus, a method, "slope splicing," was studied. Fig. 7 shows a schematic drawing of the slope splicing configuration, where the sub-mirror width is d, the slope angle of standard block 1 is Φ, and the step height h of the TSM is given by $h = d\tan\Phi$. Because $h = 20$ μm, and the sub-mirror width $d = 1$ mm, $\tan\Phi = 0.02$. The TSM manufacturing processing consists of the following procedures: material selection, polishing and cleaning; glass plates stacking and fixing; and optical surface coating.

1. Material selection: BK7 glass was used as material of glass plate.

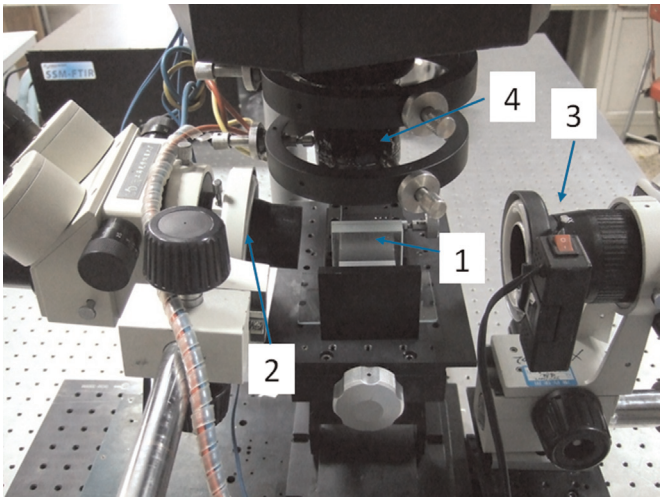

Fig. 8. Manufacturing apparatus: (1) operating equipment; (2) microscope 1; (3) microscope 2; (4) UV light source used to cure adhesive.

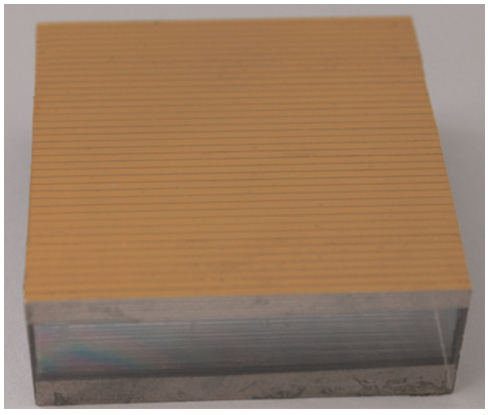

Fig. 9. Gold-coated TSM.

2. Polishing and cleaning: firstly, all of the glass plates were polished on the polishing pad at the same time, so that the demand of glass plate thickness was guaranteed. The thickness and flatness were monitored by KLA-Tencor P-16+ Surface profile and WYCO interferometer. Secondly, all glass plates were aligned with each other and temporarily consolidated. The reflecting planes were obtained by polishing one of the lateral planes of the consolidated glass plates. The size uniformity of each reflecting plane was assured by these processes. Thirdly, each glass plate was separated, then cleaned by diluted chromium acid, aceton, ethnol and deinoized water.

3. Glass plates stacking and fixing: firstly, all the glass plates were aligned and the edge of the reflecting plane touched on the standard block 1 as shown in Fig. 7. Secondly, the glass plates were pressed from two directions of horizontal and vertical, and two microscopes were used to test whether the gap between the glass plate and the standard block 1 met requirements. Thirdly, to fix all glass plates of TSM, two glass plates were respectively glued by ultraviolet (UV) light cure adhesive on two lateral faces of the TSM, then a UV light source was used to cure adhesive. Fig. 8 shows the manufacturing apparatus.

4. Optical surface coating: the structure of TSM was formed and coated with gold film as shown in Fig. 9.

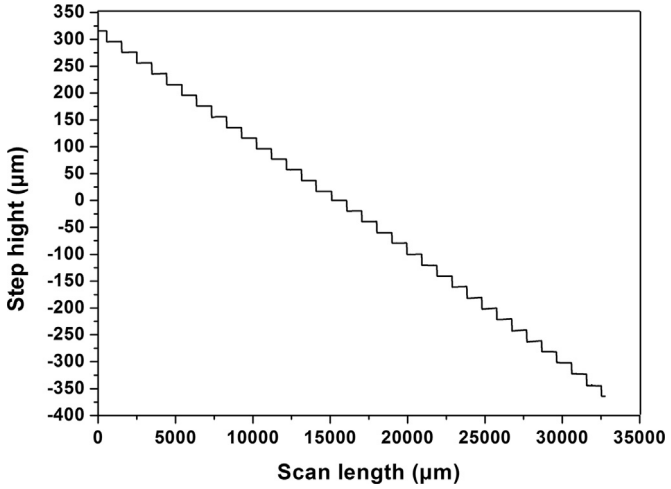

Fig. 10. Surface profile of the tall-stepped mirror tested by KLA-Tencor P-16+.

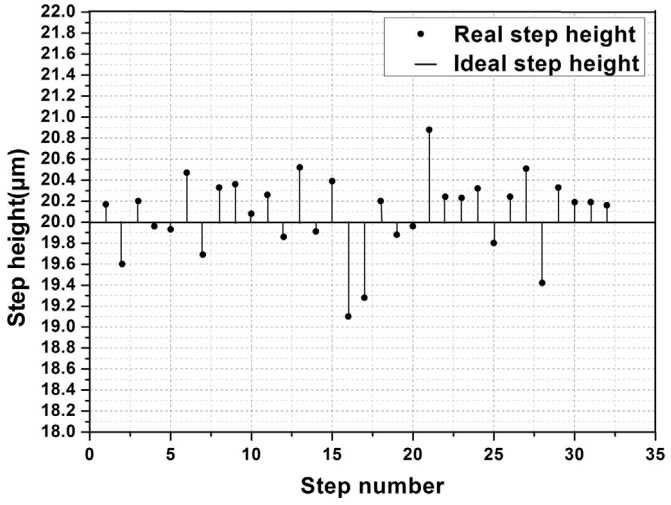

Fig. 11. Discrepancy between real step height (solid circles) and ideal step height (horizontal line).

4.2. Structural parameter testing and analysis

The step height, sub-mirror width, and sub-mirror tilt angle of TSM were tested using a KLA-Tencor P-16+ Surface profile. The surface profile is shown in Fig. 10; the scan range of the stylus tip covered the transverse distance between the lowest and highest steps, and the scan speed and scan rate were 100 μm/s and 200 Hz, respectively.

Figs. 11–13 show the discrepancy between the tested and ideal step height, sub-mirror width, and sub-mirror tilt angle, respectively. The solid circles denote the measured results, and the horizontal line denotes the ideal values.

The step height, sub-mirror width, and sub-mirror tilt angle values of the TSM obtained in the test are listed in Table 1. The value of the sub-mirror tilt angle was defined to be positive (negative) when it was tilted clockwise (counter clockwise) compared to the ideal reflective surface.

The effects of the errors in the step height, sub-mirror width, and sub-mirror tilt angle on the recovered spectrum were not independent; instead, they interacted. Therefore, we analyzed the effects of all of the errors on the recovered spectrum at the same time.

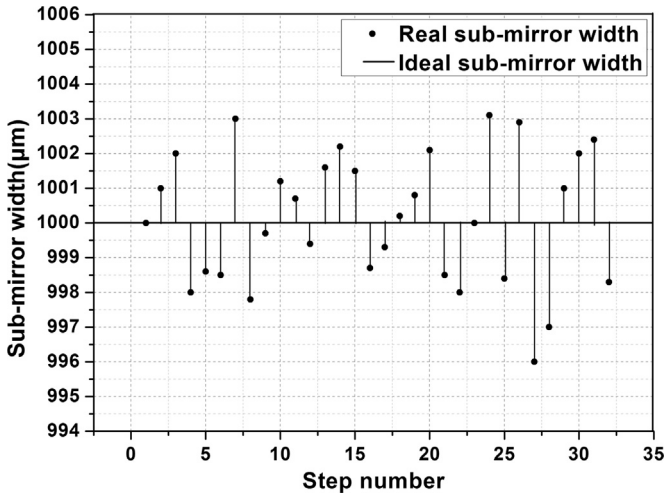

Fig. 12. Discrepancy between real sub-mirror width (solid circles) and ideal sub-mirror width (horizontal line).

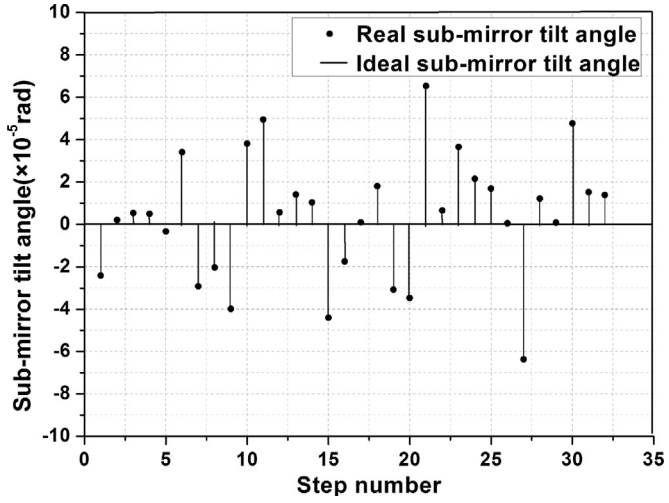

Fig. 13. Discrepancy between real sub-mirror tilt angle (solid circles) and ideal sub-mirror tilt angle (horizontal line).

Table 1
Detailed testing results for TSM.

TSM	Max.	Min.	Aver.	Standard deviation σ
Step height (μm)	20.881	19.102	20.162	0.440
Sub-mirror width (μm)	1003.102	996.014	1000.206	1.913
Sub-mirror tilt angle ($\times 10^{-5}$ rad)	6.54	−6.37	0.49	2.99

A source of discrete (SD) wavenumbers of 2100, 2300, and 2500 cm^{-1} was chosen to simulate the effects of the above three errors on the real recovered spectrum obtained by the FFT method from Eqs. (3) and (7), as shown in Fig. 14. The short-stepped mirror was considered ideally, and the SCE of the recovered spectrum, 40.67%, is large. Furthermore, the positions of all three peaks shifted toward shorter wavelengths. The intensity was weakened, and much noise was added to the spectrum.

To reduce the effect of the nonuniform samples resulting from the step height error and sub-mirror width error on the recovered spectrum, the least-squares approximation of cosine polynomials (LSC) which had been proposed by our research team and the feasibility and the stability which had been proved in [11] was

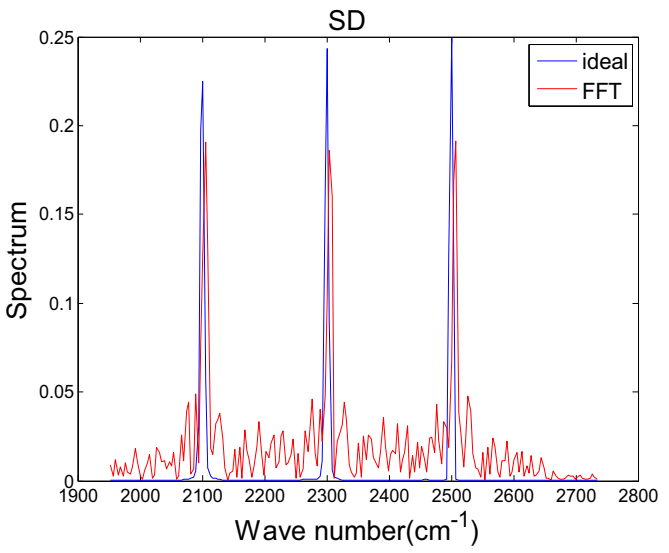

Fig. 14. Real recovered spectrum (red line) vs. the ideal spectrum (blue line) constructed by the FFT method. (For interpretation of the references to color in this figure legend, the reader is referred to the web version of this article.)

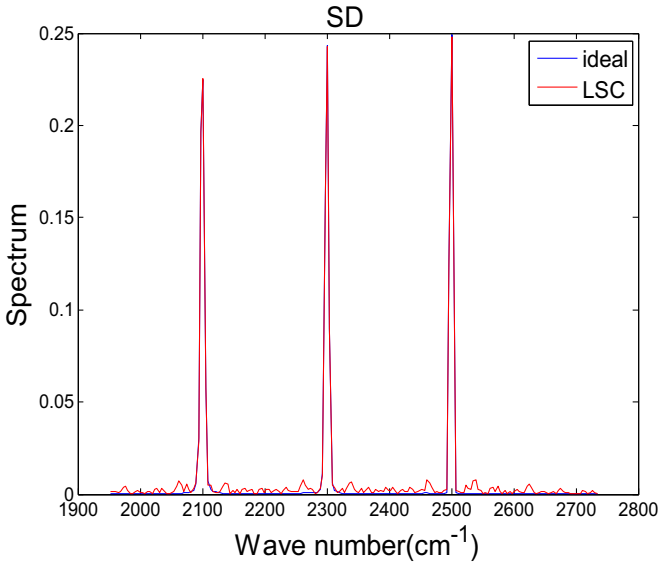

Fig. 15. Real recovered spectrum (red line) vs. the ideal spectrum (blue line) constructed by the LSC method. (For interpretation of the references to color in this figure legend, the reader is referred to the web version of this article.)

used to construct the spectrum, as shown in Fig. 15. The real recovered spectrum was obtained. Its SCE, 5.81%, meets the requirements for the system.

Note that, because the LSC method could not be used to rectify the effect of the OPD variation generated by the error in the sub-mirror tilt angle on the recovered spectrum, the real recovered spectrum is still distorted and noisy [11]. Hence, it is necessary to reduce the tilt angle effects. Further work needs to be done to optimize the conditions, including increasing the machining precision of the sub-mirror and standard block, improving the configuration to ensure more uniform pressure on the sub-mirror, and selecting a vibration-free fabrication environment.

Fig. 16 shows part of the step profile of the surface roughness tested by a WYCO interferometer. The testing results showed that the root-mean-square value of the surface roughness is 1.34 nm,

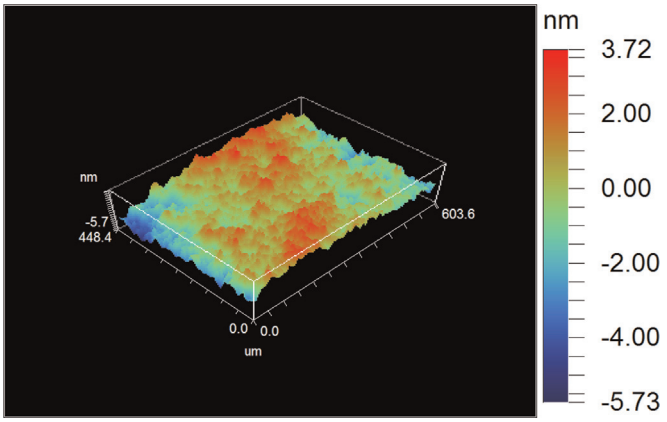

Fig. 16. Part of step profile tested by a WYCO interferometer.

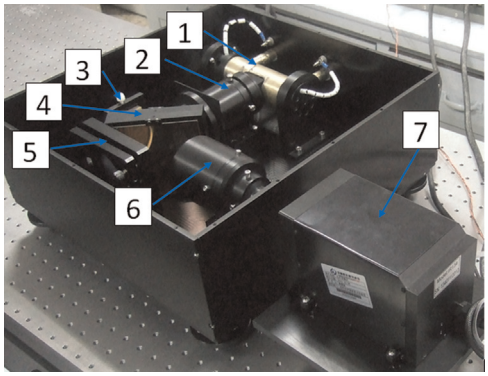

Fig. 17. Configuration of the static FTIR spectrometer. (1) Light source; (2) collimation lens; (3) tall-stepped mirror; (4) beam splitter; (5) short-stepped mirror; (6) expand lens; (7) infrared detector.

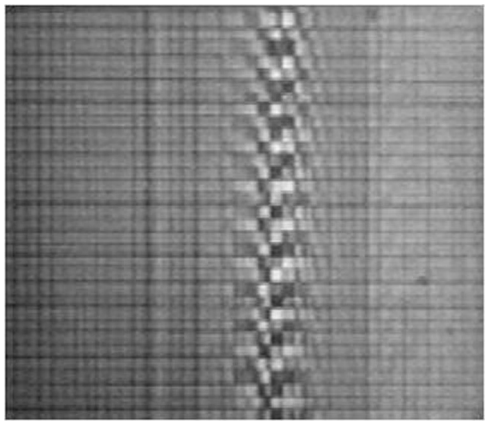

Fig. 18. Interferogram of the silicon carbide light source.

which was $5.36\times10^{-4}\,\lambda_{\min}$ ($\lambda_{\min}$=2.5 μm). Its effect on the recovered spectrum is negligible according to Fig. 6 [15].

4.3. Experiments and discussion

Experiments were performed to test the capability of TSM used in the static FTIR spectrometer in the laboratory shown as Fig. 17. In this experimental setup, a silicon carbide rod was used as the light source, and the detected spectral band was from 3.7 μm to 4.8 μm. The interferogram recorded by the detector array is shown in Fig. 18, where each square corresponds to a sample of the interferogram. This illustrates the spatial sampling produced by the stepped mirrors. Owing to the spectral width of the light

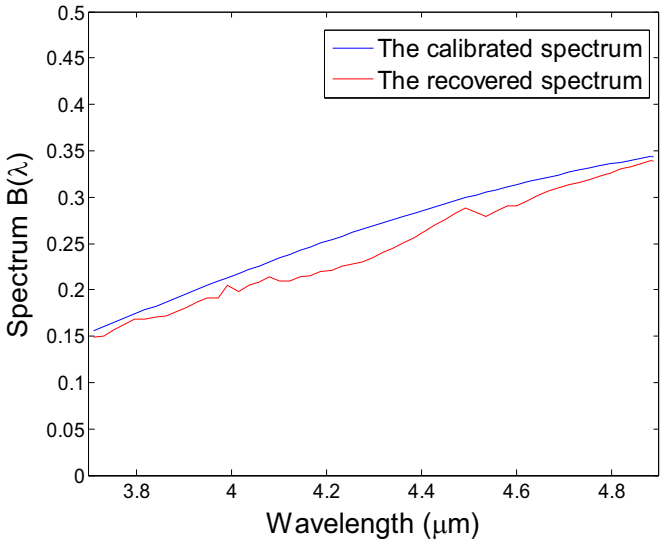

Fig. 19. Experimentally obtained recovered spectrum (red line) and calibrated spectrum (blue line). (For interpretation of the references to color in this figure legend, the reader is referred to the web version of this article.)

source, the contrast of the interferogram decreases as the OPDs increase. Fig. 19 shows the recovered spectrum (red line), which was obtained by applying various interferogram processing steps to Fig. 18, and the calibrated spectrum (blue line) obtained using an SR-5000N spectroradiometer, where the calibration temperature was 620.15 K. The position of the recovered spectrum was shifted, and much noise was added to the spectrum. The SCE of the recovered spectrum compared with the calibrated spectrum 8.76% was larger than the theory value 5.81%; in addition to the fabrication errors of the TSM, it was generated by many factors including stray light, the limited precision of the system setup, the aberration of the optical lens, and the structural parameters error of the short-stepped mirror. We believe that better experimental results can be realized by optimizing the capability of the FTIR spectrometer.

5. Conclusion

This paper presents the parameter design, fabrication process, and error analysis studies of the TSM, which is a core part of the static FTIR spectrometer. A simplicity and cost-effective slope splicing method was applied to fabricate the TSM. Testing revealed that the standard deviations of the step height, sub-mirror width, sub-mirror tilt angle, and surface roughness were 0.44 μm, 0.49 μm, 2.99×10^{-5} rad, and 1.34 nm, respectively. To solve the resulting problems of spectral distortion and noise, the LSC method was used to construct the spectrum. The SCE of the recovered spectrum decreased from 40.67% to 5.81% meets the requirements for the system and suitable for realization of a miniaturized FTIR spectrometer. In an experiment using a silicon carbide light source, the interferogram and spectrum were obtained. The SCE of the recovered spectrum compared with the calibrated spectrum 8.76% was a bit larger. Further work is necessary to optimize the capability of the system.

Acknowledgments

The authors gratefully acknowledge the support of the National Natural Science Foundation of China (Grant nos. 61376122, 61027010, 60977062, 61007023, and 20150101049JC), Science and

Technology Development Plan of Jilin Province (Grant nos. 20130206010GX, 201205025, and 20150204072GX), Changchun Science Development Plan (Grant nos. 2013261, 2011131), State Key Laboratory of Applied Optics Independent Fund and Youth Innovation promotion Association CAS (2014193).

References

[1] Qinghua Yang, Baochang Zhao, Desheng Wen, Principle and analysis of a moving double-sided mirror interferometer, Opt. Laser Technol. 44 (2012) 1256–1260.
[2] U. Wallrabe, C. Solf, J. Mohr, J.G. Korvink, Miniaturized Fourier transform spectrometer for the near infrared wavelength regime incorporating an electromagnetic linear actuator, Sens. Actuators A Phys. 123–124 (2005) 459.
[3] J.G. Lü, J.Q. Liang, Z.Z. Liang, Study on chromatic dispersion of beam splitter in spatially modulated Fourier transform spectrometer, Acta Phys. Sin. 61 (2012) 140702.
[4] C. Feng, B. Wang, Z.Z. Liang, J.Q. Liang, Miniaturization of step mirrors in a static Fourier transform spectrometer: theory and simulation, J. Opt. Soc. Am. B 28 (2011) 1–128.
[5] K.D. Möller, Miniaturized wavefront-dividing interferometers without moving parts for field and space applications, Proc. SPIE 1992 (1993) 130–139.
[6] K.D. Möller, Wave-front-dividing array interferometers without moving parts for real-time spectroscopy from the IR to the UV, Appl. Opt. 34 (1995) 9–1493.
[7] F. Brachet, P.J. Hébert, E. Cansot, C. Buil, A. Lacan, L. Roucayrol, E. Courau, F. Bernard, C. Casteras, J. Loesel, C. Pierangelo, Static Fourier transform spectroscopy breadboards for atmospheric chemistry and climate, Proc. SPIE 7100 (2008) 710019.
[8] A. Lacan, F.M. Bréon, A. Rosak, F. Brachet, L. Roucayrol, P. Etcheto, C. Casteras, Y. Salaün., A static Fourier transform spectrometer for atmospheric sounding: concept and experimental implementation, Opt. Express 18 (2010) 8–8311.
[9] E.V. Ivanov, Static Fourier transform spectroscopy with enhanced resolving power, J. Opt A. Pure Appl. Opt. 2 (2000) 6–519.
[10] Y.M. Kong, J.Q. Liang, Z.Z. Liang, B. Wang, J. Zhang, Micro assembled Fourier transform spectrometer, Proc. SPIE 7283 (2009) 728304.
[11] C. Feng, J.Q. Liang, Z.Z. Liang, Spectrum constructing with nonuniform samples using least-squares approximation by cosine polynomials, Appl. Opt. 50 (2011) 34–6377.
[12] L. Palchetti, D. Lastrucci, Spectral noise due to sampling errors in Fourier-transform spectroscopy, Appl. Opt. 40 (2001) 19–3235.
[13] P.R. Griffiths, J.A. de Haseth, "Signal-to-noise ratio", Fourier Transform Infrared Spectrometry, Wiley & Sons, 2007, pp. 167–168.
[14] J.G. Lü, J.Q. Liang, Z.Z. Liang, Error synthesis and statistical analysis on stepped mirror array by Monte Carlo method, Acta Phys. Sin. 61 (2012) 22–220701.
[15] Y. Zheng, J.Q. Liang, Z.Z. Liang, Design and fabrication of step mirrors used in space-modulated Fourier transform infrared spectrometer, Opt. Express 21 (2013) 1–884.
[16] B. Wang, Z.Z. Liang, Y.M. Kong, J.Q. Liang, J.G. Fu, Y. Zheng, W.B. Zhu, J.G. Lü, W. Wang, B.P. Shu, J. Zhang, Design and fabrication of micro multi-mirrors based on siliconfor micro-spectrometer, Acta Phys. Sin. 59 (2010) 907–912.